Preparation of PEGylated liposomes incorporating lipophilic lomeguatrib derivatives for the sensitization of chemo-resistant gliomas

Signorell, Rea D ; Papachristodoulou, Alexandros ; Xiao, Jiawen ; Arpagaus, Bianca ; Casalini, Tommaso ; Grandjean, Joanes ; Thamm, Jana ; Steiniger, Frank ; Luciani, Paola ; Brambilla, Davide ; Werner, Beat ; Martin, Ernst ; Weller, Michael ; Roth, Patrick ; Leroux, Jean-Christophe

Abstract: Liposomal delivery is a well-established approach to increase the therapeutic index of drugs, mainly in the field of cancer chemotherapy. Here, we report the preparation and characterization of a new liposomal formulation of a derivative of lomeguatrib, a potent O6-methylguanine-DNA methyltransferase (MGMT) inactivator. The drug had been tested in clinical trials to revert chemoresistance, but was associated with a low therapeutic index. A series of lomeguatrib conjugates with distinct alkyl chain lengths - i.e. C12, C14, C16, and C18 - was synthesized, and the MGMT depleting activity as well as cytotoxicity were determined on relevant mouse and human glioma cell lines. Drug-containing liposomes were prepared and characterized in terms of loading and in vitro release kinetics. The lipophilic lomeguatrib conjugates did not exert cytotoxic effects at 5 M in the mouse glioma cell line and exhibited a similar MGMT depleting activity pattern as lomeguatrib. Overall, drug loading could be improved by up to 50-fold with the lipophilic conjugates, and the slowest leakage was achieved with the C18 derivative. The present data show the applicability of lipophilic lomeguatrib derivatization for incorporation into liposomes, and identify the C18 derivative as the lead compound for in vivo studies.

DOI: https://doi.org/10.1016/j.ijpharm.2017.11.070

Preparation of PEGylated liposomes incorporating lipophilic lomeguatrib derivatives for the sensitization of chemo-resistant gliomas

Authors: Rea D. Signorell[1], Alex Papachristodoulou[2], Jiawen Xiao[1], Bianca Arpagaus[1], Tommaso Casalini[3,4], Joanes Grandjean[5], Jana Thamm[6], Frank Steiniger[7], Paola Luciani[1,6], Davide Brambilla[1], Patrick Roth[2], Beat Werner[8], Ernst Martin[8], Michael Weller[2] & Jean-Christophe Leroux[1]

[1] Institute of Pharmaceutical Sciences, Department of Chemistry and Applied Biosciences, ETH Zurich, 8093 Zurich, Switzerland

[2] Laboratory of Molecular Neuro-oncology, University Hospital Zurich, 8091 Zurich, Switzerland

[3] Institute for Chemical and Bioengineering, Department of Chemistry and Applied Biosciences, ETH Zurich, 8093 Zurich, Switzerland

[4] Institute of Mechanical Engineering and Material Technology, Department of Innovative Technology, SUPSI, 6928 Manno, Switzerland

[5] Institute for Biomedical Engineering, Department of Information Technology and Electrical Engineering, UZH & ETH Zurich, 8093 Zurich, Switzerland

[6] Institute of Pharmacy, Department of Pharmaceutical Technology, Friedrich Schiller University Jena, 07743 Jena, Germany

[7] Electron Microscopy Center, University Hospital Jena, Friedrich-Schiller-University Jena, 07743 Jena, Germany

[8] Zentrum für MR-Forschung, University Children's Hospital, 8032 Zurich, Switzerland

PL current address: Institute of Pharmacy, Department of Pharmaceutical Technology, Friedrich Schiller University Jena, 07743 Jena, Germany.

DB current address: Faculty of Pharmacy, University of Montreal, H3T 1J4 Montreal, QC, Canada.

Abstract

Liposomal delivery is a well-established approach to increase the therapeutic index of drugs, mainly in the field of cancer chemotherapy. The implementation of remote loading techniques has enabled high encapsulation yields and prolonged retention of ionizable and membrane-permeable drugs. However, polar or amphiphobic drugs with low molecular weight still represent a challenge and suffer from poor entrapment efficiencies. This obstacle can be overcome by means of lipophilic derivatization, which enables effective anchoring of the drug in the phospholipid bilayer. Here, we report the preparation and characterization of a new liposomal formulation of a derivative of lomeguatrib, a potent O^6-methylguanine-DNA methyltransferase (MGMT) inactivator. The drug had been tested in clinical trials to revert chemoresistance, but was associated with a low therapeutic index. A series of lomeguatrib conjugates with distinct alkyl chain lengths – *i.e.* C12, C14, C16, and C18 – were synthesized, and their cytotoxicity as well as MGMT depletion activity were determined on relevant mouse and human glioma cell lines. Drug-containing liposomes were prepared and characterized in terms of loading and *in vitro* release kinetics. Except for the C12 derivative, the lipophilic lomeguatrib derivatives did not exert cytotoxic effects at 5 μM in the mouse glioma cell line, and exhibited a similar MGMT depletion activity pattern as lomeguatrib. Overall, drug loading could be improved by up to 50-fold with the lipophilic conjugates, and the slowest leakage was achieved with the C18 derivative. The present data show the applicability of lipophilic lomeguatrib derivatization for incorporation into liposomes, and identify the C18 derivative as the lead compound for *in vivo* studies.

Keywords: methylguanine-DNA methyltransferase inactivators, lomeguatrib, liposomes, lipophilic derivatives, drug loading, liposomal retention

Abbreviations: BBB, blood-brain barrier; Br-Cn, bromoalkane; Br-C12, 1-bromododecane; Br-C14, 1-bromotetradecane; Br-C16, 1-bromohexadecane; Br-C18, 1-bromooctadecane; CHOL, cholesterol; DCM, dichloromethane; DLS, dynamic light scattering; DMEM, Dulbecco's modified Eagle's medium; DMF, dimethylformamide; DMSO, dimethyl sulfoxide; DOPC, 1,2-dioleoyl-*sn*-glycero-3-phosphocholine; DSC, differential scanning calorimetry; DSPE-PEG, N-(carbonyl-methoxypolyethylenglycol-2000)-1,2-distearoyl-*sn*-glycero-3-phosphoethanolamine, Na-salt; EDTA, ethylenediaminetetraacetic acid; EPR-effect, enhanced permeation and retention effect; FBS, fetal bovine serum; HEPES, 4-(2-hydroxyethyl)piperazine-1-ethanesulfonic acid; horseradish peroxidase, HRP; LiH, lithium hydride; MGMT, O^6-methylguanine-DNA methyltransferase; MLV, multilamellar vesicle;

O^6BG, O^6-benzylguanine; O^6BTG, O^6-(4-bromothenyl)guanine; O^6BTG-C8-Glu, 8-[O^6-(4-bromothenyl)-guan-9-yl]-octyl-*β*-D-glucoside; O^6BTG-Cn, synthesized lipophilic derivatives of O^6BTG; PDI, polydispersity index; PBS, phosphate-buffered saline; SEC, size exclusion chromatography; SD, standard deviation; TEM, transmission electron microscopy; Tris, tris(hydroxymethyl)aminomethane; UV, ultraviolet.

1. Introduction

Liposomes have successfully been used as carriers to ameliorate the therapeutic index of chemotherapeutic drugs such as doxorubicin, daunorubicin and more recently vincristine and irinotecan (Gill et al., 1996; Ko et al., 2011; O'Brien et al., 2010; O'Brien et al., 2004). Passive as well as active loading methods allow the encapsulation of a broad range of drugs, from hydrophilic to amphiphilic and lipophilic molecules, in either the hydrophilic aqueous core or the surrounding phospholipid lipid bilayer. While the entrapment of polar drugs is often associated with low efficiency, it can be improved substantially by remote loading procedures as long as the compounds are ionizable and sufficiently membrane–permeable, which is the case with several notable examples on the market such as doxorubicin and vincristine sulfate liposomes (Doxil® or Marqibo®, respectively) (Boman et al., 1993; Haran et al., 1993; Mayer et al., 1990). Some classes of molecules, however, remain difficult to load into liposomes. For example, non-glycosylated purine analogues are mostly insoluble in water and show only marginal solubility in organic solvents. Gulati *et al.* termed this class of amphiphobic compounds as "biphasic insoluble drugs" (Gulati et al., 1998). Indeed, the biphasic insoluble nature of drugs like allopurinol, 8-azaguanine, and 6-mercaptopurine makes them challenging candidates for liposomal formulations, as neither interactions with the lipid bilayer nor stable retention in the inner core can be achieved (Fendler and Romero, 1976; Liautard et al., 1991; Taneja et al., 2000).

Lipophilic derivatization is an effective strategy for the improvement of drug loading in liposomes (Gabizon et al., 2006) that has enabled formulations with increased drug entrapment by several thousand-fold (Sasaki et al., 1987; Tokunaga et al., 1988). In this process, a lipophilic anchor is covalently conjugated to the drug of interest, often *via* biodegradable linkers (*e.g.* ester, disulfide), which dock the pharmaceutical active component at the liposomal bilayer.

Lomeguatrib (or O^6BTG, short for O^6-(4-bromothenyl)guanine) is a purine analogue with biphasic insoluble properties, and a potent inactivator and pseudo-substrate of the O^6-methylguanine-DNA methyltransferase (MGMT). Firstly synthesized in the early 90's, O^6BTG showed greater *in vitro* potency compared to O^6-benzylguanine (O^6BG), the very first MGMT inactivator tested in humans. Clinically, O^6BTG has been evaluated for its ability to counteract MGMT-induced resistance against triazene-based chemotherapeutics such as temozolomide (Ranson et al., 2006) and dacarbazine (Tawbi et al., 2011). Unfortunately, O^6BTG potentiated the hematological toxicity of alkylating antineoplastic agents at effective dosage, a downside shared with several other MGMT inactivators, which precluded any advantage over the treatment with antineoplastic agent alone (Kefford et al., 2009; Khan et al., 2008; Ranson et al., 2006; Sabharwal et al., 2010). In the early 2000s, the group of Wiessler addressed the drug's tumor-specificity and aqueous solubility by linking glucose to O^6BTG (Reinhard et al., 2001a; Reinhard et al., 2001b). The authors examined the ability of a series of conjugates to inactivate MGMT as a function of spacer length, revealing that a minimum of 8 carbon atoms (C8) in the spacer arm were required for adequate depletion activity. Nonetheless, their lead compound, 8-[O^6-(4-bromothenyl)-guan-9-yl]-octyl-β-D-glucoside (O^6BTG-C8-Glu), induced higher cytotoxicity than O^6BTG. While information regarding the water-solubility of O^6BTG-C8-Glu was not provided in the study, the strong hydrophobic character of the linker would suggest that only a small solubility improvement was achieved. Given the hematological toxicity of O^6BTG in humans when combined with alkylating agents, we hypothesized that the incorporation of O^6BTG into liposomes could improve the drug's therapeutic index by altering its biodistribution profile. Capitalizing on the benefits of long-circulating poly(ethylene glycol)-modified liposomes, the proposed approach could enhance drug deposition in tumors exhibiting an innate enhanced permeability and retention (EPR) effect. Moreover,O^6BTG-loaded liposomes could also constitute a valid therapeutic strategy for challenging neoplasms largely lacking an EPR effect (Gao et al., 2013), *e.g.* glioblastoma multiforme, provided strategies to locally permeabilize the BBB are put in place, such as microbubble-enhanced focused ultrasound (FUS) (Treat et al., 2007; Treat et al., 2012).

In this work, the development of a liposomal formulation of O^6BTG suitable for parenteral administration is described. A series of alkylated O^6BTG derivatives (O^6BTG-Cn) was synthesized with chain lengths ranging from C12 to C18 with the aim of increasing O^6BTG loading in liposomes. The impact of the lipophilic anchor conjugation on the derivatives' MGMT depleting activity and cytotoxic properties were assessed in temozolomide-resistant

glioma cells. Furthermore, liposomes loaded with the O^6BTG derivatives were prepared and characterized. Based on the obtained experimental results, a promising lead formulation with highly favorable *in vitro* performance was identified for *in vivo* studies.

2. Materials and Methods

2.1 Materials

Chloroform, cholesterol (CHOL), dimethyl sulfoxide (DMSO), ethanol, ethyl acetate, ethylenediaminetetraacetic acid (EDTA), 4-(2-hydroxyethyl)piperazine-1-ethanesulfonic acid (HEPES), horseradish peroxidase (HRP), methanol, O^6BG, silica gel, tris(hydroxymethyl)aminomethane (Tris) base, polysorbate 20, sodium phosphate dibasic heptahydrate, and sodium phosphate monobasic monohydrate were purchased from Sigma-Aldrich Chemie GmbH (Buchs, Switzerland). Anhydrous dimethylformamide (DMF) was supplied by Acros Organics (Geel, Belgium) and dichloromethane (DCM) by Fisher Scientific (Reinach, Switzerland). O^6BTG and O^6BTG-C8-Glu were bought from Cayman Chemical (Ann Arbor, MI). Lithium hydride (LiH), 1-bromododecane (Br-C12; purity 98%) as well as 1-bromooctadecane (Br-C18; purity 97%) were purchased from abcr GmbH (Karlsruhe, Germany) and 1-bromotetradecane (Br-C14; purity ≥ 97%) as well as 1-bromotetradecane (Br-C16; purity ≥ 96%) were supplied by Merck Millipore KGaA (Darmstadt, Germany). 1,2-dioleoyl-*sn*-glycero-3-phosphocholine (DOPC) and N-(carbonyl-methoxypolyethylenglycol-2000)-1,2-distearoyl-*sn*-glycero-3-phosphoethanolamine, Na-salt (DSPE-PEG) were bought from Lipoid GmbH (Ludwigshafen am Rhein, Germany). Tris-HCl was purchased from Axon Lab AG (Baden-Dättwil, Switzerland). The murine glioma cell line SMA-497 was derived from a spontaneous astrocytoma in a VM/Dk mouse as previously characterized (Ahmad et al., 2014; Fraser, 1971) and kindly provided by Dr. D. Bigner (Duke University, School of Medicine, Durham, NC). The human malignant glioma cell line LN-18, previously described by Bartussek *et al.* (Bartussek et al., 1999), was kindly provided by Dr. N. de Tribolet (Centre Hospitalier Universitaire Vaudois, Lausanne, Switzerland). Phosphate-buffered saline (PBS), Dulbecco's modified Eagle's medium (DMEM, high glucose, pyruvate, no glutamine), DMEM (high glucose, no glutamine, no phenol red), and L-glutamine were purchased from Life Technologies (Zug, Switzerland). Anti-human MGMT antibody, fetal bovine serum (FBS), NP40 cell lysis buffer, and skim milk were bought from Thermo Fisher Scientific AG (Reinach, Switzerland). Anti-mouse MGMT antibody was

purchased from R&D Systems (Minneapolis, MN). Anti-*β*-actin antibody, goat anti-rat IgG-HRP antibody, and donkey anti-goat IgG-HRP antibody were purchased from Santa Cruz Biotechnologies (Santa Cruz, CA). Sheep anti-mouse IgG-HRP antibody was bought from GE Healthcare Life Sciences (Chalfont St Giles, UK).

2.2 Synthesis of O^6BTG derivatives

The synthesis of lipophilic O^6BTG derivatives (O^6BTG-Cn) was adapted after Kjellberg *et al.* and Reinhard *et al.* (**Fig. 1**) (Kjellberg et al., 1986; Reinhard et al., 2001b). Briefly, LiH (9.7 mg, 1.23 mmol) was suspended in 6.5 mL anhydrous DMF, added to 200 mg O^6BTG (0.613 mmol) under inert atmosphere and the temperature increased to 80 °C under constant stirring. Subsequently, 0.613 mmol of the respective bromoalkane (Br-Cn; Br-C12: 152.8 mg, Br-C14: 170.0 mg, Br-C16: 187.2 mg, Br-C18: 204.4 mg) were dissolved in 4.8 mL anhydrous DMF and dropwise added to the reaction mixture and left under stirring for 3 h at 80 °C. After equilibrating to room temperature, 6.5 mL phosphate buffer (100 mM, pH 7) were added dropwise to stop the reaction and left stirring for further 15 min. The products were extracted 3 times with chloroform and the combined organic phases were concentrated under reduced pressure at 70 °C. Purification by column chromatography on silica gel base employing gradient elution with ethyl acetate/DCM/ethanol (10:10:1 v/v/v) and DCM/methanol (10:1 v/v) allowed the separation of N9 and N7 isomers yielding white solids. Analysis of O^6BTG-Cn was performed by ^{1}H-NMR and ^{13}C-NMR spectroscopies on a Bruker Ultra Shield at 400 MHz (Bruker, Karlsruhe, Germany). High resolution mass spectrometry (HRMS)-ESI was performed on a maXis UHR-TOF mass spectrometer (Bruker) by the MS service of ETHZ. Melting points of the synthesized isomers were determined by differential scanning calorimetry (DSC) at heating rates of 10 °C/min with a Q200 DSC System (TA Instruments, Eschborn, Germany) under nitrogen atmosphere using Tzero aluminium hermetic pans (TA Instruments).

2.3 Cell culture

SMA-497 mouse glioma cells and LN-18 human glioma cells were grown in complete medium (DMEM supplemented with 10% FBS and 2 mM L-glutamine) in a humidified atmosphere of 5% CO_2 at 37 °C and routinely passaged 2-3 times per week. For cytotoxicity

and MGMT depleting experiments, cells were grown to about 80% confluence before use. Both cell lines were regularly tested for the absence of mycoplasma. More specific culture conditions are given in the respective sections.

2.4 MGMT depleting activity of O^6BTG-Cn

The MGMT depleting activity of the O^6BTG-Cn derivatives was assessed by Western blot adapting a protocol from Towbin *et al.* (Towbin et al., 1979). Cells (2 x 10^5 per well) were seeded in 6-well plates, grown for 24 h and exposed to increasing concentrations of O^6BTG-Cn (N9) for another 24 h. The medium was then replaced and after 72 h the cells were lysed with lysis buffer (25 mM Tris-HCl, 120 mM sodium chloride, 5 mM EDTA, 0.5% NP40 cell lysis buffer) (Seystahl et al., 2015). Total protein (30 µg/lane) was separated on a 12% acrylamide gel. After transfer to nitrocellulose membranes, the blots were blocked for 1 h in 5% milk-Tris-buffered saline with polysorbate 20, and incubated overnight at 4 °C with the respective primary antibodies (anti-human MGMT, anti-murine MGMT or anti-*β*-actin). The membranes were then washed and incubated with secondary antibodies conjugated to HRP (sheep anti-mouse IgG-HRP, goat anti-rat IgG-HRP, and donkey anti-goat IgG-HRP) at room temperature for 1 h. Protein bands were detected using enhanced chemiluminescence by a Curix 60 table-top processor (Agfa, Mortsel, Belgium).

2.5 Cytotoxicity experiments

The cytotoxic potential of O^6BTG-Cns was determined *in vitro* using a MTS assay (CellTiter® 96 Aqueous Non-Radioactive Cell Proliferation Assay, Promega, Madison, WI) according to manufacturer's instructions. More specifically, SMA-497 and LN-18 cells were seeded at a density of 1 x 10^4 cells/well in 100 µL of complete medium in a 96-well plate and allowed to adhere for 24 h. The medium was then changed with 100 µL serum-free medium with 1% of DMSO containing increasing concentrations of either O^6BG, O^6BTG, O^6BTG-C8-Glu, O^6BTG-Cn (0, 1.25, 2.5, 5, 10, 20, and 40 µM). After 24 h, the medium was replaced by 100 µL phenol red-, serum-free DMEM and 20 µL CellTiter 96®AQ_{ueous} One Solution Reagent. The cells were incubated for 2 h to reduce the MTS tetrazolium compound into a reddish formazan product, which was subsequently quantified by spectrophotometry at 490 nm with an Infinite M200Pro plate reader (Tecan, Maennedorf, Switzerland).

2.6 Preparation of drug-loaded liposomes

Small unilamellar liposomes were prepared by the lipid film hydration/extrusion method (Hope et al., 1985). More specifically, chloroform stock solutions of DOPC, CHOL and DSPE-PEG were mixed at a molar ratio of 72.5:20:7.5. O^6BG and O^6BTG-C8-Glu were dissolved in the mixed lipid solution at a drug-to-lipid ratio of 4 mol%, while O^6BTG and the respective O^6BTG-Cn were dissolved to gain drug-to-lipid ratios of 1, 2.5, 3, 4, 5 and 7.5 mol%. In the cases of O^6BG, O^6BTG and O^6BTG-C8-Glu, a mixture of chloroform and methanol (80:20 v/v final ratio) was needed for complete compound dissolution. The solvents were removed under reduced pressure at 60 °C, and the lipid film was stored under vacuum overnight. Rehydration of the lipid film was performed with PBS under vigorous vortexing at room temperature to give a final lipid concentration of 100 mM. The liposomes were extruded 10 times through polycarbonate membranes of 0.05 μm pore size at room temperature using a Lipex 10 mL extruder (Lipex Biomembranes, Burnaby, BC, Canada), sterile filtered, and kept at 4 °C for a maximum of 5 days until use. Hydrodynamic diameters and PDIs were measured by DLS (intensity-average) using a Delsa Nano C particle analyzer (Beckman Coulter, Brea, CA).

2.7 Cryo-transmission electron microscopy (cryo-TEM)

Five μL of each sample was applied to a copper grid covered by holey carbon film (Quantifoil Multi A Micro Tools GmbH, Jena, Germany) and excess of liquid was blotted automatically between two strips of filter paper. Subsequently, the samples were rapidly plunged into liquid ethane (cooled to ~ 180 °C) in a cryobox (Carl Zeiss NTS GmbH, Oberkochen, Germany). Excess ethane was removed with a piece of filter paper. The samples were transferred immediately with a Gatan 626 cryo-transfer holder (Gatan, Pleasanton, CA) into the pre-cooled cryo-electron microscope (Philips CM 120, Eindhoven, Netherlands) operated at 120 kV and viewed under low dose conditions. The images were recorded with a 2k CMOS Camera (F216, TVIPS, Gauting, Germany). In order to minimize the noise, four images were recorded and averaged to one image.

2.8 Determination of drug loading

Liposomal loading was initially measured after removing free drug by size exclusion chromatography (SEC) with prepacked PD-10 desalting columns (GE Healthcare Life Sciences, Chalfont St Giles, UK) for O^6BG, O^6BTG, O^6BTG-C8-Glu, and all O^6BTG-Cn. However, in further experiments SEC was omitted for all O^6BTG-Cn due to their low partitioning into the aqueous phase, as further specified in their elution profiles presented in the Supplementary Information (**S.1**). Drug concentration in the liposome suspension was assessed by UV spectrophotometry using an Infinite M200Pro plate reader. Briefly, liposomes were diluted 1:50 in methanol and measured at a test wavelength of 286 nm against a reference wavelength of 350 nm to account for methanol interference. Equally diluted empty liposomes were used as blank. The drug concentration in the liposome suspensions was normalized to its phosphate content determined by a molybdane blue-based phosphate assay after conversion to inorganic phosphate (Morrison, 1964).

2.9 In vitro release kinetics

Drug release from liposomes was determined *in vitro* following a protocol developed by Shabbits *et al.* (2002). This assay is based on the transfer of lipophilic drugs from donor drug-containing liposomes to acceptor multilamellar vesicles (MLVs) mimicking the *in vivo* drug transfer rate to hydrophobic pools. Briefly, donor O^6BTG-Cn-loaded liposomes were incubated with acceptor MLVs at a 1:100 mol ratio in 4-(2-hydroxyethyl)piperazine-1-ethanesulfonic acid (HEPES)-buffered saline for 24 h at 37 °C under constant stirring. Samples were withdrawn at various times (0, 0.5, 1, 2, 4, 8, and 24 h) and centrifuged at 1600 x *g* for 10 min to separate acceptor MLVs from donor liposomes, which remained in the supernatant. The drug amount in the supernatant was assessed by high-performance liquid chromatography (HPLC). Details on MLV preparation and drug quantification by HPLC are available as Supplementary Information (**S.2**).

2.10 Statistical analysis

Statistics were performed with SigmaPlot 13.0 software (Systat Software Inc., San Jose, CA). All data presented are means ± SD of at least three independent samples. One-way ANOVA combined with a Tukey test for pairwise comparison was performed to distinguish differences between test groups defining a p value of ≤ 0.05 as statistically significant.

3. Results and discussion

3.1 Synthesis of O⁶BTG derivatives

The alkylation of O^{6}BTG (**Fig. 1**) was a one-step synthesis with a yield of ca. 80% for the isomeric mixture (**Table 1**). O^{6}BTG-Cn were prepared from the respective Br-Cn and O^{6}BTG *via* nucleophilic substitution, yielding two different isomers at the respective N7 or N9 position of the guanine moiety. The structures of all O^{6}BTG-Cn (N7 and N9) were determined by ^{1}H-NMR and ^{13}C-NMR spectroscopies (Supplementary Information: **S.3**). Melting points obtained by DSC were in the range of 112 to 122 °C for the N7 derivatives, and in the range of 99 to 105 °C for the N9 derivatives (**Table 1**). An increase in chain length led to a decrease in melting points in the N7 isomers, whereas the opposite trend was recorded for the N9 isomers. Both the melting entropy and enthalpy generally increased with increasing chain lengths. For the alkyl chains of the N9 isomer it might, however, be easier to establish van der Waals interactions due to a larger distance to the bromothenyl-residue compared to the N7 isomer. Ordered domains may attenuate the increase in melting entropy as a function of chain length, making the increase in melting enthalpy the dominating factor for the N9 and leading to a rise in melting points (Zhang et al., 2014; Zhang and Maginn, 2014). With regard to the N7, the enthalpy increase compared to the one of the N9 might be reduced, resulting in a melting point decrease. As previously observed by Kjellberg *et al.,* the chosen synthetic strategy favored the N9 isomer (Kjellberg et al., 1986).

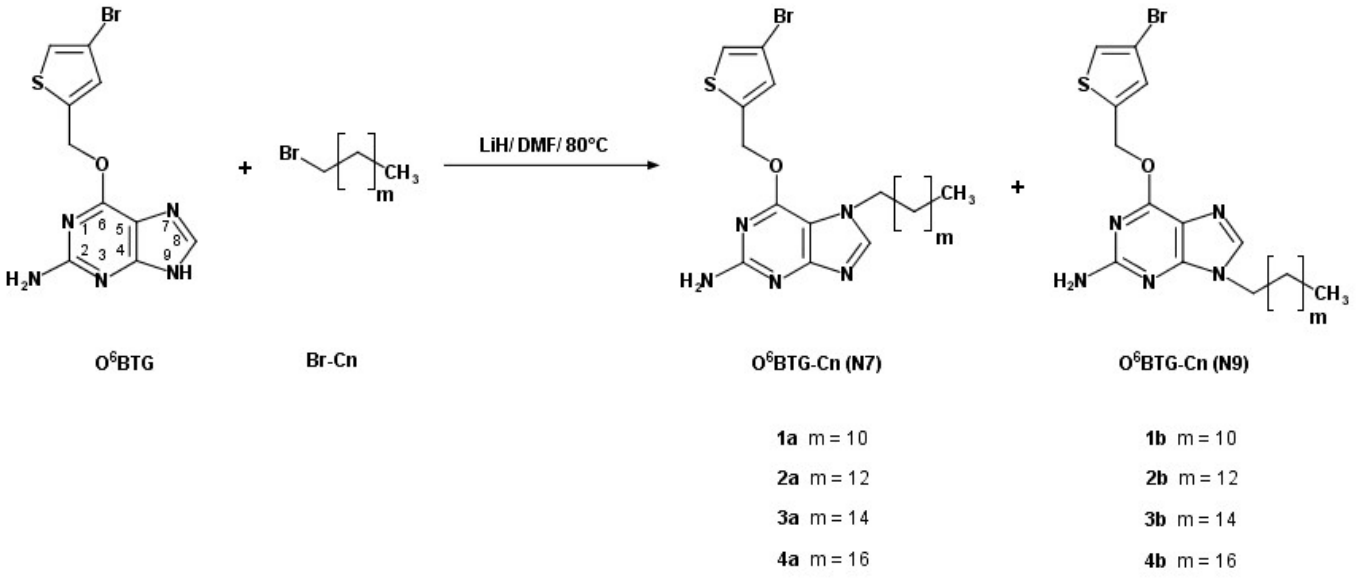

Fig. 1. Synthesis scheme of O^{6}BTG-Cn.

Table 1. List of synthesized O^6BTG-Cn.

Compound	Abbreviation	Yield (%)	T_m (°C)
O^6-(4-bromothenyl)-7-dodecylguanine (**1a**)	O^6BTG-C12 (N7)	23	122
O^6-(4-bromothenyl)-9-dodecylguanine (**1b**)	O^6BTG-C12 (N9)	54	99
O^6-(4-bromothenyl)-7-tetradecylguanine (**2a**)	O^6BTG-C14 (N7)	27	118
O^6-(4-bromothenyl)-9-tetradecylguanine (**2b**)	O^6BTG-C14 (N9)	57	101
O^6-(4-bromothenyl)-7-hexadecylguanine (**3a**)	O^6BTG-C16 (N7)	27	118
O^6-(4-bromothenyl)-9-hexadecylguanine (**3b**)	O^6BTG-C16 (N9)	56	103
O^6-(4-bromothenyl)-7-octadecylguanine (**4a**)	O^6BTG-C18 (N7)	24	112
O^6-(4-bromothenyl)-9-octadecylguanine (**4b**)	O^6BTG-C18 (N9)	57	105

3.3 MGMT depleting activity of O^6BTG-Cn

Several former studies evaluating alternative O^6BTG derivatives have reported that N7-substitution of MGMT inactivators consistently resulted in complete loss of MGMT depleting activity (Chae et al., 1994; Moschel et al., 1992). Based on these findings, we investigated the depleting activity of one N7 isomer, O^6BTG-C12 (N7), and compared it to its N9 counterpart. A direct comparison of the two isomers in SMA-497 glioma cells (**Fig. 2**) revealed that the N9 was more active than the N7. Indeed, the N7 isomer did not show any significant depletion on SMA-497 cells in the tested concentration range. These results confirmed previous work (Chae et al., 1994; Moschel et al., 1992), and might be explained by the structural similarity between the N9 isomer and the natural target of MGMT, the DNA, in which the nitrogen atom at position 9 of the guanine base is linked to the 1' carbon atom of the deoxyribose.

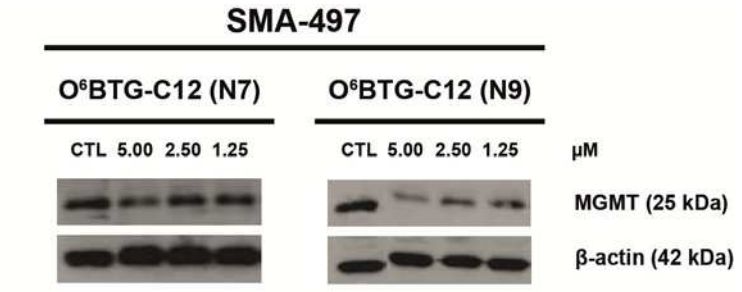

Fig. 2. MGMT inactivation by O^6BTG-C12 (N7 and N9) in SMA-497 glioma cells by representative Western blot images. The untreated 100% control is abbreviated by CTL.

To understand the isomer-dependent depleting activity, we investigated the isomers' binding mechanisms to MGMT using molecular dynamics (MD) simulations. Chemical reactions between the protein and the ligand were not investigated, since this requires a more complex simulation protocol which would go beyond the purpose of this work. The binding site of human MGMT with O^6BG was used for binding studies with O^6BTG and O^6BTG-C12 (N7 and N9) (Wibley et al., 1995; Wibley et al., 2000). Indeed, the binding mechanism of the active part of the N9 isomer was analogous to the one of O^6BTG (**Figs. 3A, B**); in addition, the arrangement of the alkyl chain was consistent with the findings reported for O^6BTG-C8-Glu (N9) by Reinhard et al. (Reinhard et al., 2001c). Interestingly, the N7 isomer also exhibited a similar pose within the binding pocket (**Fig. 3C**), but the binding stability was dependent on the orientation of the aliphatic chain. Unbinding events that destabilized the protein-ligand interaction were found when the alkyl chain was oriented similarly to the one of the N9 isomer as illustrated in **Fig. 3D**. However, stable binding is most likely a prerequisite for the covalent reaction between protein and MGMT inhibitors, explaining the poor MGMT depleting activity of the N7 isomer. An additional set of simulations was performed for O^6BTG-C18 (N7 and N9); molecular trajectories showed a behavior analogous to O^6BTG-C12 isomers. A detailed discussion of the performed MD simulations is provided in the Supporting Information (**S.4**).

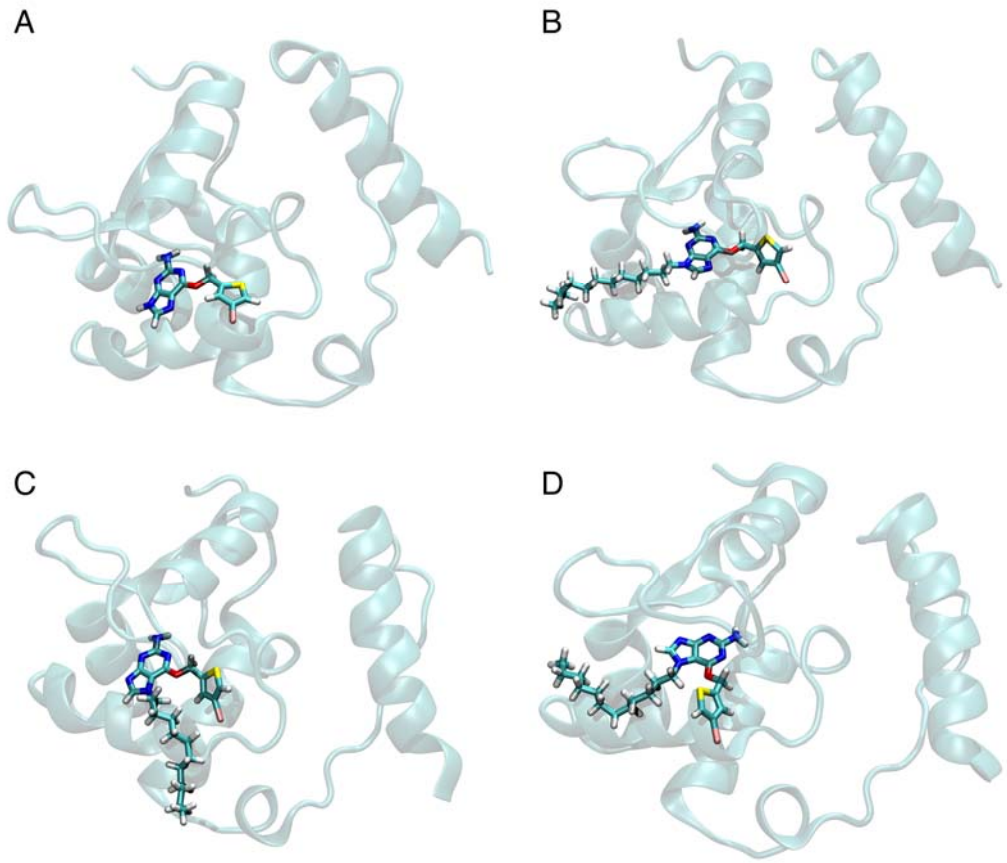

Fig. 3. Representative MGMT binding poses of O^6BTG (A), O^6BTG-C12 (N9) (B) and O^6BTG-C12 (N7) (C). Unbinding event of O^6BTG-C12 (N7) (D).

Given the confirmed superior MGMT depleting effect, the N9 derivatives were selected for all further experiments.

The impact of the alkyl chain length on the drug activity of the N9 isomers was then evaluated by monitoring the levels of intracellular MGMT protein levels on SMA-497 and LN-18 cells at increasing O^6BTG-Cn concentrations. As illustrated in **Fig. 4**, all derivatives inactivated MGMT in a concentration-dependent manner and depleted MGMT with a similar potency as O^6BTG on both tested cell lines. Interestingly, O^6BTG as well as O^6BTG-Cn appeared to have a stronger MGMT depletion effect on the human-derived cell line LN-18 than on the mouse-derived one SMA-497. Possibly, interspecies variability of the MGMT protein led to different affinities for the same purine analog (Crone et al., 1994).

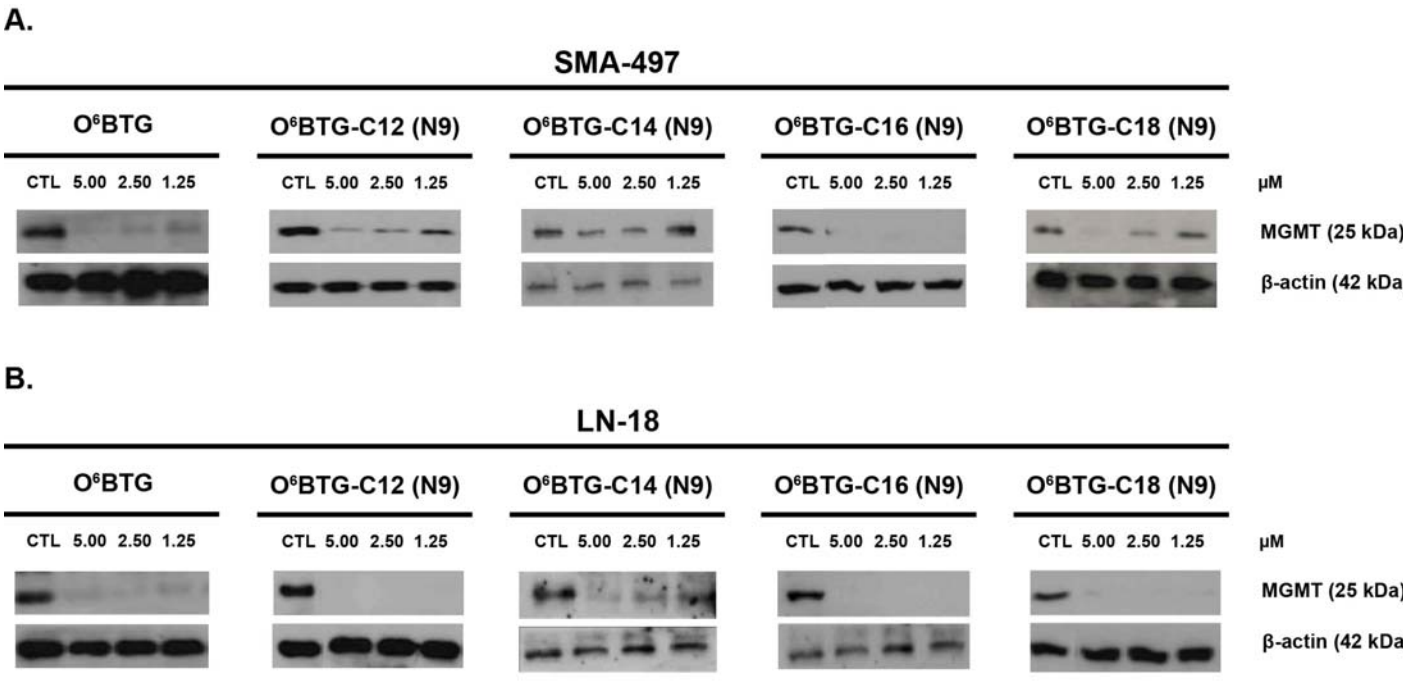

Fig. 4. MGMT depletion by O^6BTG and O^6BTG-Cn (N9) in SMA-497 (A) and LN-18 glioma cells (B) at different concentrations, indicated by representative Western blot images. The untreated 100% control is abbreviated CTL.

3.2 In vitro cytotoxicity of O^6BTG-Cn (N9)

The cytotoxicity of the O^6BTG-Cn (N9) derivatives was assessed in murine SMA-497 and human LN-18 cells, and compared to those of the parent drug and two established MGMT inactivators, namely O^6BG and O^6BTG-C8-Glu. Similar to the parent drug, a concentration-dependent decrease of cell viability was found for all derivatives in both cell lines, with a more prominent effect in LN-18 cells (**Figs. 5 A-D**). Although MGMT inactivators are not expected to be highly cytotoxic given that their target protein does not hold – to current knowledge – housekeeping tasks in the cell (Margison et al., 2003; Tsuzuki et al., 1996), off-target cytotoxicity can occur. Remarkably, aside from O^6BTG-C12, all derivatives showed low cytotoxicity in the SMA-497 cell line. On the other hand, in LN-18 cells O^6BTG-C12, O^6BTG-C14 and O^6BTG-C16 induced a strong decrease in cell viability after a 24 h incubation period at a 40 μM concentration, reaching 25% survival for O^6BTG-C12 (**Fig. 5 D**). O^6BTG-C18, the derivative with the longest alkyl chain, did not show prominent toxicity in the tested concentration range, and was in fact significantly less toxic than O^6BTG at 10-40 μM in SMA-497 cells and 5-20 μM in LN-18 cells (**Figs. 5 B, D**). It is noteworthy that toxic effects appeared to be inversely related to the alkyl chain length in both cell lines. Given

their strong lipophilic nature, the O^6BTG-Cn derivatives might bear a greater potential to permeate biological membranes than the parent drug O^6BTG, making them more likely to reach the intracellular space. With regard to the alkyl chain length, derivatives with longer chains might associate with plasma membranes more strongly, minimizing further transfer to subcellular compartments and, in turn decreasing cytotoxic effects as demonstrated for O^6BTG-C18 (Locatelli et al., 2008). Nevertheless, as emphasized in section 3.3, enough O^6BTG-C18 molecules may still gain access to the cell and efficiently deplete MGMT. Based on its low cytotoxic potential compared to the parent compound and the other O^6BTG-Cn, O^6BTG-C18 may thus represent a suitable alternative for a potentially non-toxic AGT inactivation *in vivo*.

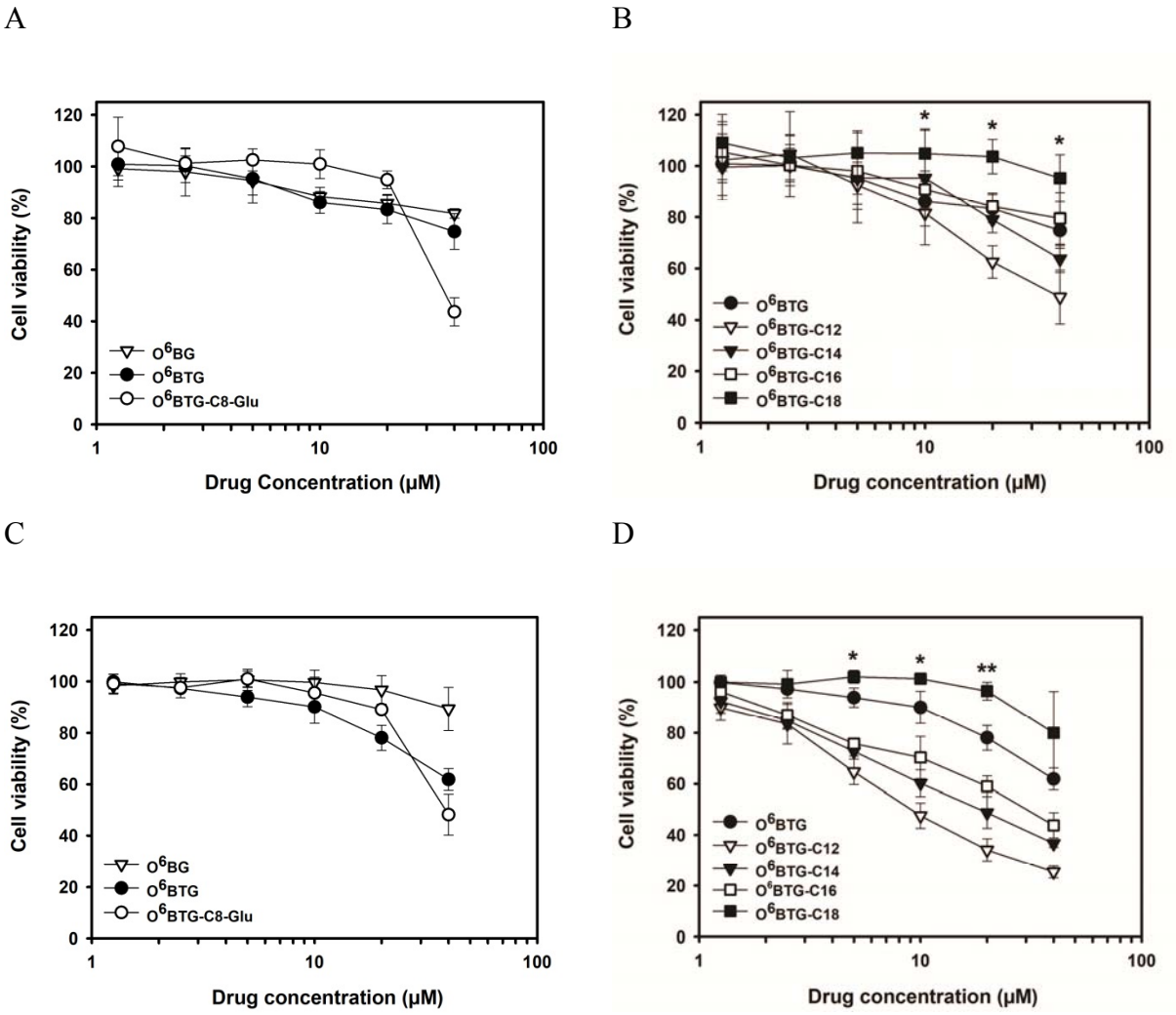

Fig. 5. Cell viability data of SMA-497 (A, B) and LN-18 cells (C, D) after incubation with established MGMT inactivators and with O^6BTG-Cn, respectively. Data for O^6BTG are illustrated in both panels, respectively. Data are means ± SD (n = 3), $^{*}p \leq 0.05$, $^{**}p \leq 0.01$ O^6BTG-C18 vs. O^6BTG.

3.6 Characterization and drug loading of liposomal O^6BTG-Cn formulations

The different O^6BTG-Cn were passively loaded into DOPC-based liposomes using the lipid film hydration method followed by extrusion. Empty and drug-loaded liposomes had a mean hydrodynamic diameter of ca. 75 nm with a PDI below 0.2 (Supplementary Information: **S.5**). Considering that tumoral deposition depends on nanoparticle size, the obtained hydrodynamic diameter might be suitable for passive delivery *via* the EPR effect alone or preferably in combination with localized BBB permeabilization, for instance with microbubble-enhanced FUS (Sunoqrot et al., 2014; Treat et al., 2007). Cryo-TEM-based images of empty and O^6BTG-C18-loaded liposomes (4 mol%) showed mainly spherical unilamellar particles with very few bi-lamellar and invaginated liposomes (**Fig. 6**). No drug precipitates were apparent in the recorded images.

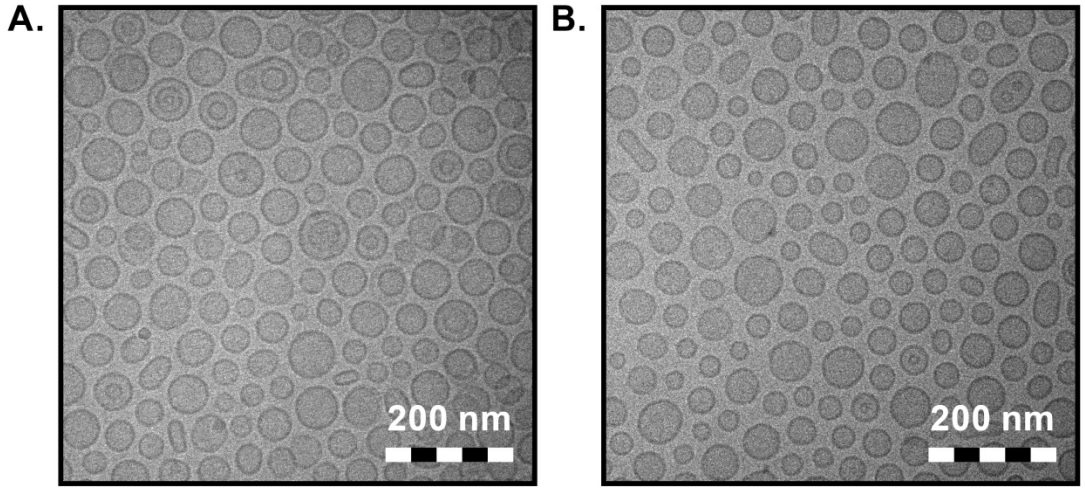

Fig. 6. Cryo-TEM images of (A) empty and (B) O^6BTG-C18-loaded liposomes at a drug loading of 4 mol%.

Drug loadings of O^6BG, O^6BTG, O^6BTG-C8-Glu, and O^6BTG-Cn were measured and compared at an initially added drug concentration of 4 mol% (**Fig. 7**). O^6BG and O^6BTG revealed loadings of <0.02 mol% and 0.08 ± 0.03 mol%, respectively, with entrapment efficiencies below or equal to 2%. The use of O^6BTG conjugated to an octyl-glucose linker led to a 10-fold increase in drug loading (0.87 ± 0.13 mol%), likely a result of a stronger hydrophobic interaction of the C8-moiety with the liposomal bilayer. O^6BTG conjugations with simple alkyl chains gave rise to significantly increased loadings, reaching entrapment efficiencies of more than 85%.

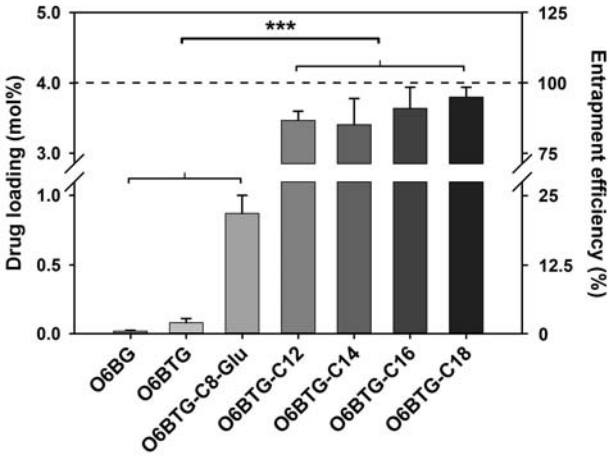

Fig. 7. Drug loading of different MGMT inactivators after SEC. Data are means ± SD ($n = 3$), $^{***}p \leq 0.001$.

Having established the superior drug loading of the lipophilic derivatives over O^6BTG, the maximum loading capacity was determined. Due to the extremely low aqueous solubility of the alkylated compounds, the liposomes were only purified by eliminating the precipitated, unentrapped O^6BTG-Cn *via* filtration during the extrusion procedure. Maximum drug loading was reached at the initially added drug concentrations of 4 and 5 mol% (**Fig. 8**). Above these concentrations, the formulations were not stable, as evidenced by the formation of precipitates within 24 h (data not shown), which reflected the oversaturation of the system. At an initial N9) by Reinhard et al. □ ADDIN EN.CITE □ ADDIN EN.CITE.DATA □□□□(□ HYPERLINK \l "_ ENREF_29" \o "Reinhard, 2001 #1114" □□Reinhard et al., 2001c□)□. Interestin[g]ly, the N7 iso mer also exhibited a similar pose within the binding pocket (Fig.cal lipid chain length of O^6BTG-C18 and the main liposomal lipid. With up to 50-fold higher loading compared to the parent drug, similar drug loading behaviors were observed with all O^6BTG-Cn.

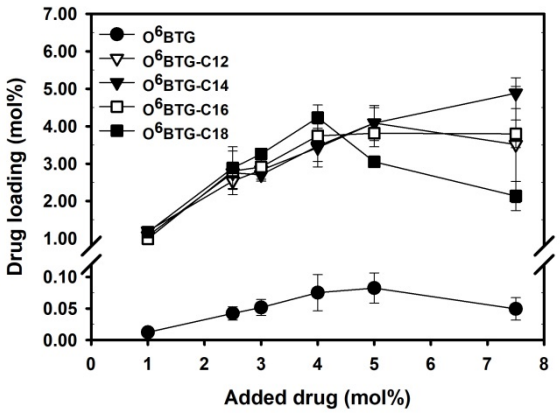

Fig. 8. Drug loading curves of O^6BTG, O^6BTG-C12, O^6BTG-C14, O^6BTG-C16, and O^6BTG-C18. Data are means ± SD ($n = 3$).

3.7 Liposomal drug retention in vitro

The release kinetics of the liposomal formulation was monitored *in vitro* over 24 h at 37 °C with an assay using MLVs as acceptor compartment (Shabbits et al., 2002). The release rates correlated with the alkyl chain length (**Fig. 9**). The O^6BTG-C12 and O^6BTG-C14 derivatives were transferred very quickly to the surrounding MLVs and already after 1 h, more than 60% of the loaded drug had distributed to the MLV population. O^6BTG-C16 was transferred to an extent lower than 30% within the same time frame, while with O^6BTG-C18 the drug retention was much higher and less than 40 and 60% of the C18 derivative was released after 8 h and 24 h, respectively.

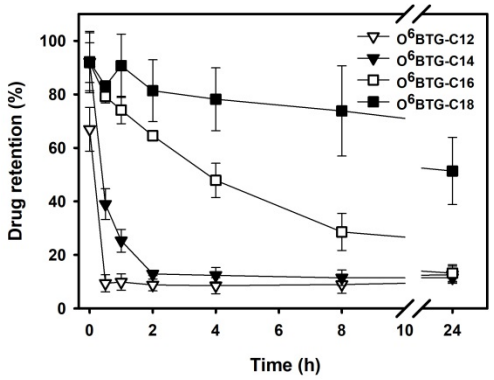

Fig. 9. Drug retention profiles of different O^6BTG-Cn in liposomes. Data are means ± SD (n = 3-4).

The improved liposomal retention observed for O^6BTG-Cn with longer alkyl chains can be attributed to an increase of hydrophobic interactions with the lipid bilayer, which would stabilize the drugs' anchoring (Shabbits et al., 2002). It is important to mention that the alkyl chain length of O^6BTG-C18 is identical to the main lipid of our liposomal formulation, DOPC, which might minimize membrane perturbation while enhancing membrane embedding for this derivative.

With regard to a future *in vivo* application, the incorporation of O^6BTG-C18 into long-circulating PEGylated liposomes may be suitable for the enhancement of the drug's biological half-life, a prerequisite for improved tumor deposition, while ensuring sustained release at the tumoral site.

Conclusion

This study presents several novel long-circulating liposomal formulations of MGMT inactivator derivatives that may increase the tumor deposition *via* the EPR-effect and/or after localized BBB permeabilization. Given the marginal liposomal loading of highly potent but low tumor-specific MGMT inactivators such as O^6BG and O^6BTG, lipophilic drug derivatization was utilized to increase liposomal incorporation. The MGMT depleting activity of O^6BTG was preserved in the lipophilic conjugates, and especially in the derivative with the longest alkyl chain length (C18), which did not exhibit conspicuous cytotoxicity, and was in fact less toxic than O^6BTG. The sustained drug retention of O^6BTG-C18 in PEGylated liposomes in combination with the long-circulating behavior of the carrier can alter the drug's biodistribution and improve its *in vivo* performance, making this liposomal formulation an eligible candidate for future MGMT-induced chemoresistant tumor therapies. The strategy described could potentially be used for other guanine-based MGMT inactivators in the future. Studies evaluating the *in vivo* efficacy of O^6BTG-C18-based liposomes in a glioma-bearing rodent animal model together with temozolomide are currently ongoing.

Acknowledgements

This work was financially supported by the Swiss National Foundation (Sinergia program, CRSII3_147651). Lipoid GmbH is acknowledged for the endowment to the University of Jena (P. L.). The authors thank Jong Ah Kim for critical reading and editing of the manuscript. The authors acknowledge the computational resources provided by Euler Cluster at ETH Zurich. T. C. acknowledges the contribution of Ms. Michela Castelnuovo for image editing.

References

Ahmad, M., Frei, K., Willscher, E., Stefanski, A., Kaulich, K., Roth, P., Stühler, K., Reifenberger, G., Binder, H., Weller, M., 2014. How Stemlike Are Sphere Cultures From Long-term Cancer Cell Lines? Lessons From Mouse Glioma Models. Journal of Neuropathology & Experimental Neurology 73, 1062-1077.

Bartussek, C., Naumann, U., Weller, M., 1999. Accumulation of Mutant p53V143A Modulates the Growth, Clonogenicity, and Radiochemosensitivity of Malignant Glioma Cells Independent of Endogenous p53 Status. Experimental Cell Research 253, 432-439.

Boman, N.L., Mayer, L.D., Cullis, P.R., 1993. Optimization of the retention properties of vincristine in liposomal systems. Biochimica et Biophysica Acta (BBA) - Biomembranes 1152, 253-258.

Chae, M.Y., McDougall, M.G., Dolan, M.E., Swenn, K., Pegg, A.E., Moschel, R.C., 1994. Substituted O6-Benzylguanine Derivatives and Their Inactivation of Human O6-Alkylguanine-DNA Alkyltransferase. Journal of Medicinal Chemistry 37, 342-347.
Crone, T.M., Goodtzova, K., Edara, S., Pegg, A.E., 1994. Mutations in Human O6-Alkylguanine-DNA Alkyltransferase Imparting Resistance to O6-Benzylguanine. Cancer Research 54, 6221-6227.
Fendler, J.H., Romero, A., 1976. Encapsulation of 8-azaguanine in single multiple compartment liposomes. Life Sciences 18, 1453-1458.
Fraser, H., 1971. Astrocytomas in an inbred mouse strain. The Journal of Pathology 103, 266-270.
Gabizon, A.A., Tzemach, D., Horowitz, A.T., Shmeeda, H., Yeh, J., Zalipsky, S., 2006. Reduced Toxicity and Superior Therapeutic Activity of a Mitomycin C Lipid-Based Prodrug Incorporated in Pegylated Liposomes. Clinical Cancer Research 12, 1913-1920.
Gao, H., Pang, Z., Jiang, X., 2013. Targeted Delivery of Nano-Therapeutics for Major Disorders of the Central Nervous System. Pharm Res 30, 2485-2498.
Gill, P.S., Wernz, J., Scadden, D.T., Cohen, P., Mukwaya, G.M., Roenn, J.H.v., Jacobs, M., Kempin, S., Silverberg, I., Gonzales, G., Rarick, M.U., Myers, A.M., Shepherd, F., Sawka, C., Pike, M.C., Ross, M.E., 1996. Randomized phase III trial of liposomal daunorubicin versus doxorubicin, bleomycin, and vincristine in AIDS-related Kaposi's sarcoma. Journal of Clinical Oncology 14, 2353-2364.
Gulati, M., Grover, M., Singh, S., Singh, M., 1998. Lipophilic drug derivatives in liposomes. Int. J. Pharm. 165, 129-168.
Haran, G., Cohen, R., Bar, L.K., Barenholz, Y., 1993. Transmembrane ammonium sulfate gradients in liposomes produce efficient and stable entrapment of amphipathic weak bases. Biochimica et Biophysica Acta (BBA) - Biomembranes 1151, 201-215.
Hope, M.J., Bally, M.B., Webb, G., Cullis, P.R., 1985. Production of large unilamellar vesicles by a rapid extrusion procedure. Characterization of size distribution, trapped volume and ability to maintain a membrane potential. Biochimica et Biophysica Acta (BBA) - Biomembranes 812, 55-65.
Kefford, R.F., Thomas, N.P.B., Corrie, P.G., Palmer, C., Abdi, E., Kotasek, D., Beith, J., Ranson, M., Mortimer, P., Watson, A.J., Margison, G.P., Middleton, M.R., 2009. A phase I study of extended dosing with lomeguatrib with temozolomide in patients with advanced melanoma. Br J Cancer 100, 1245-1249.
Khan, O.A., Ranson, M., Michael, M., Olver, I., Levitt, N.C., Mortimer, P., Watson, A.J., Margison, G.P., Midgley, R., Middleton, M.R., 2008. A phase II trial of lomeguatrib and temozolomide in metastatic colorectal cancer. Br J Cancer 98, 1614-1618.
Kjellberg, J., Liljenberg, M., Johansson, N.G., 1986. Regioselective alkylation of 6-(β-methoxyethoxy)guanine to give the 9-alkylguanine derivative. Tetrahedron Letters 27, 877-880.
Ko, A.H., Tempero, M.A., Shan, Y., Su, W., Lin, Y., Dito, E., Ong, A., Yeh, G., Chen, L., 2011. A multinational phase II study of liposome irinotecan (PEP02) for patients with gemcitabine-refractory metastatic pancreatic cancer. Journal of Clinical Oncology 29, 237-237.
Liautard, J., Philippot, J.R., Liautard, J.P., 1991. Encapsulation of drugs into large unilamellar liposomes prepared by an extemporaneous method. Journal of Microencapsulation 8, 381-389.
Locatelli, C., Rosso, R., Santos-Silva, M.C., de Souza, C.A., Licínio, M.A., Leal, P., Bazzo, M.L., Yunes, R.A., Creczynski–Pasa, T.B., 2008. Ester derivatives of gallic acid with potential toxicity toward L1210 leukemia cells. Bioorganic & Medicinal Chemistry 16, 3791-3799.
Margison, G.P., Povey, A.C., Kaina, B., Santibáñez Koref, M.F., 2003. Variability and regulation of O6-alkylguanine–DNA alkyltransferase. Carcinogenesis 24, 625-635.
Mayer, L.D., Tai, L.C.L., Bally, M.B., Mitilenes, G.N., Ginsberg, R.S., Cullis, P.R., 1990. Characterization of liposomal systems containing doxorubicin entrapped in response to pH gradients. Biochimica et Biophysica Acta (BBA) - Biomembranes 1025, 143-151.
Morrison, W.R., 1964. A fast, simple and reliable method for the microdetermination of phosphorus in biological materials. Analytical Biochemistry 7, 218-224.
Moschel, R.C., McDougall, M.G., Dolan, M.E., Stine, L., Pegg, A.E., 1992. Structural features of substituted purine derivatives compatible with depletion of human O6-alkylguanine-DNA alkyltransferase. Journal of Medicinal Chemistry 35, 4486-4491.

O'Brien, S.M., Aulitzky, W., Yehuda, D.B., Lister, J., Schiller, G.J., Seiter, K., Smith, S.E., Stock, W., Silverman, J.A., Kantarjian, H., 2010. Phase II study of marqibo in adult patients with refractory or relapsed philadelphia chromosome negative (Ph-) acute lymphoblastic leukemia (ALL). Journal of Clinical Oncology 28, 6507-6507.
O'Brien, M.E.R., Wigler, N., Inbar, M., Rosso, R., Grischke, E., Santoro, A., Catane, R., Kieback, D.G., Tomczak, P., Ackland, S.P., Orlandi, F., Mellars, L., Alland, L., Tendler, C., 2004. Reduced cardiotoxicity and comparable efficacy in a phase III trial of pegylated liposomal doxorubicin HCl (CAELYX™/Doxil®) versus conventional doxorubicin for first-line treatment of metastatic breast cancer. Annals of Oncology 15, 440-449.
Ranson, M., Middleton, M.R., Bridgewater, J., Lee, S.M., Dawson, M., Jowle, D., Halbert, G., Waller, S., McGrath, H., Gumbrell, L., McElhinney, R.S., Donnelly, D., McMurry, T.B.H., Margison, G.P., 2006. Lomeguatrib, a Potent Inhibitor of O⁶-Alkylguanine-DNA-Alkyltransferase: Phase I Safety, Pharmacodynamic, and Pharmacokinetic Trial and Evaluation in Combination with Temozolomide in Patients with Advanced Solid Tumors. Clinical Cancer Research 12, 1577-1584.
Reinhard, J., Eichhorn, U., Wiessler, M., Kaina, B., 2001a. Inactivation of O6-methylguanine-DNA methyltransferase by glucose-conjugated inhibitors. Int. J. Cancer 93, 373-379.
Reinhard, J., Hull, W.E., von der Lieth, C.-W., Eichhorn, U., Kliem, H.-C., Kaina, B., Wiessler, M., 2001b. Monosaccharide-Linked Inhibitors of O6-Methylguanine-DNA Methyltransferase (MGMT): Synthesis, Molecular Modeling, and Structure−Activity Relationships. Journal of Medicinal Chemistry 44, 4050-4061.
Reinhard, J., Hull, W.E., von der Lieth, C.W., Eichhorn, U., Kliem, H.C., Kaina, B., Wiessler, M., 2001c. Monosaccharide-linked inhibitors of O-6-methylguanine-DNA methyltransferase (MGMT): Synthesis, molecular modeling, and structure-activity relationships. J Med Chem 44, 4050-4061.
Sabharwal, A., Corrie, P.G., Midgley, R.S., Palmer, C., Brady, J., Mortimer, P., Watson, A.J., Margison, G.P., Middleton, M.R., 2010. A phase I trial of lomeguatrib and irinotecan in metastatic colorectal cancer. Cancer Chemother. Pharmacol. 66, 829-835.
Sasaki, H., Matsukawa, Y., Hashida, M., Sezaki, H., 1987. Characterization of alkylcarbamoyl derivatives of 5-fluorouracil and their application to liposome. Int. J. Pharm. 36, 147-156.
Seystahl, K., Tritschler, I., Szabo, E., Tabatabai, G., Weller, M., 2015. Differential regulation of TGF-β–induced, ALK-5–mediated VEGF release by SMAD2/3 versus SMAD1/5/8 signaling in glioblastoma. Neuro-Oncology 17, 254-265.
Shabbits, J.A., Chiu, G.N.C., Mayer, L.D., 2002. Development of an in vitro drug release assay that accurately predicts in vivo drug retention for liposome-based delivery systems. J. Control. Release 84, 161-170.
Sunoqrot, S., Bugno, J., Lantvit, D., Burdette, J.E., Hong, S., 2014. Prolonged blood circulation and enhanced tumor accumulation of folate-targeted dendrimer-polymer hybrid nanoparticles. J. Control. Release 191, 115-122.
Taneja, D., Namdeo, A., Mishra, P.R., Khopade, A.J., Jain, N.K., 2000. High-Entrapment Liposomes for 6-Mercaptopurine—A Prodrug Approach. Drug Development and Industrial Pharmacy 26, 1315-1319.
Tawbi, H.A., Villaruz, L., Tarhini, A., Moschos, S., Sulecki, M., Viverette, F., Shipe-Spotloe, J., Radkowski, R., Kirkwood, J.M., 2011. Inhibition of DNA repair with MGMT pseudosubstrates: phase I study of lomeguatrib in combination with dacarbazine in patients with advanced melanoma and other solid tumours. Br J Cancer 105, 773-777.
Tokunaga, Y., Iwasa, T., Fujisaki, J., Sawai, S., Kagayama, A., 1988. Liposomal Sustained-Release Delivery Systems for Intravenous Injection. IV. : Antitumor Activity of Newly Synthesized Lipophilic 1-β-D-Arabinofuranosylcytosine Prodrug-Bearing Liposomes. CHEMICAL & PHARMACEUTICAL BULLETIN 36, 3574-3583.
Towbin, H., Staehelin, T., Gordon, J., 1979. Electrophoretic transfer of proteins from polyacrylamide gels to nitrocellulose sheets: procedure and some applications. Proc. Natl. Acad. Sci. 76, 4350-4354.
Treat, L.H., McDannold, N., Vykhodtseva, N., Zhang, Y., Tam, K., Hynynen, K., 2007. Targeted delivery of doxorubicin to the rat brain at therapeutic levels using MRI-guided focused ultrasound. Int. J. Cancer 121, 901-907.

Treat, L.H., McDannold, N., Zhang, Y., Vykhodtseva, N., Hynynen, K., 2012. Improved Anti-Tumor Effect of Liposomal Doxorubicin After Targeted Blood-Brain Barrier Disruption by MRI-Guided Focused Ultrasound in Rat Glioma. Ultrasound in Medicine & Biology 38, 1716-1725.
Tsuzuki, T., Kunihiko, S., Shiraishi, A., Kawate, H., Igarashi, H., Iwakuma, T., Tominaga, Y., Zhang, S., Shimizu, S., Ishikawa, T., Nakamura, K., Nakao, K., Katsuki, M., Sekiguchi, M., 1996. Targeted disruption of the DNA repair methyltransferase gene renders mice hypersensitive to alkylating agent. Carcinogenesis 17, 1215-1220.
Wibley, J.E., McKie, J.H., Embrey, K., Marks, D.S., Douglas, K.T., Moore, M.H., Moody, P.C., 1995. A homology model of the three-dimensional structure of human O6-alkylguanine-DNA alkyltransferase based on the crystal structure of the C-terminal domain of the Ada protein from Escherichia coli. Anti-cancer drug design 10, 75-95.
Wibley, J.E.A., Pegg, A.E., Moody, P.C.E., 2000. Crystal structure of the human O6-alkylguanine-DNA alkyltransferase. Nucleic Acids Research 28, 393-401.
Zhang, H., Ma, X., Cao, C., Wang, M., Zhu, Y., 2014. Multifunctional iron oxide/silk-fibroin (Fe 3 O 4–SF) composite microspheres for the delivery of cancer therapeutics. RSC Advances 4, 41572-41577.
Zhang, Y., Maginn, E.J., 2014. Molecular dynamics study of the effect of alkyl chain length on melting points of [CnMIM][PF6] ionic liquids. Physical Chemistry Chemical Physics 16, 13489-13499.